Desalination and Water Treatment
www.deswater.com

doi:10.5004/dwt.2017.20625

76 (2017) 241–253
May

Synthesis of magnetic nanohybrid of Fe^{3+}-TMSPT-MNPs as a novel adsorbent: Optimization of Cr(VI) adsorption by response surface methodology

Nasibeh Nikraftar, Farshid Ghorbani*

Department of Environmental Science, Faculty of Natural Resource, University of Kurdistan, 66177-15177, Sanandaj, Iran, email: n.nikraftar@yahoo.com (N. Nikraftar), Tel. +98 8733620551, Fax +988733620550, email: farshidghorbani59@yahoo.com, f.ghorbani@ uok.ac.ir (F. Ghorbani)

Received 28 July 2016; Accepted 25 February 2017

ABSTRACT

The adsorptive removal of Cr(VI) using magnetic nanohybrid of Fe^{3+}-TMSPT-MNPs as a novel adsorbent has been investigated. In this regards, magnetic Fe_3O_4 nanoparticles (MNPs) were synthesized by the sol-gel method and then modified by 3-(trimethoxysilyl)-1-propanethiol and ferric chloride. The structural features of the produced materials were characterized by means of XRD, N_2 adsorption-desorption, FT-IR, VSM and SEM. Central composite design (CCD) under response surface methodology (RSM) was applied to the design of the experiments to maximize Cr(VI) removal from aqueous solutions. More specifically, the effects of pH, temperature, chromium ion concentration and sorbent dosage were investigated on the chromium adsorption. A total of 20 sets of experiments were designed by the software to achieve maximum removal efficiency (R). The significance of the independent variables and model were tested by the analysis of variance (ANOVA). The best local maximum values for pH, Cr(VI) concentration and sorbent dosage were found to be 4.28, 30 $mg{\cdot}L^{-1}$ and 2 $g{\cdot}L^{-1}$, respectively, that yielded maximum R of 62.10%. Furthermore, the obtained value for desirability was equal to 0.945. The results indicated that the equilibrium data are well fitted by the Freundlich model. Additionally, the kinetic data are analyzed well by the pseudo-second-order model with a high correlation coefficient. The thermodynamic study illustrated the feasibility, spontaneous and exothermic nature of the adsorption process.

Keywords: Adsorption; Fe_3O_4; Magnetic nanohybrid; Chromium; Response surface methodology

1. Introduction

In many countries water contamination with heavy metals has become a serious problem. Chromium is a highly toxic metal that exists usually in water bodies in two oxidation states of Cr(III) and Cr(VI). Hexavalent chromium is more toxic than trivalent chromium due to its high water solubility and mobility, as well as strong oxidizing nature of the Cr(VI) which can lead to carcinogenic and mutagenic effects [1–3]. Cr(VI) is usually released into the environment from various industrial effluents such as, leather tanning, electroplating, paint, paper, pulp production and ore and petroleum refining [4,5]. The United States Environmental Protection Agency (usEPA) and World Health Organization (WHO) have limited the amount for Cr(VI) concentration in drinking water at 0.1 and 0.05 $mg{\cdot}L^{-1}$, respectively [6]. Therefore, the removal of Cr(VI) from industrial wastewaters before discharge into the environment is very important.

In this regard, a variety of methods have been used for the removal of Cr(VI) from water and wastewaters including adsorption [7], ion-exchange [8], coagulation [9], reduction [2], membrane separation [10], etc. Among these processes, adsorption is one of the more popular and widely used methods due to simplicity, easiness of handling, availability of wide range of adsorbents and its efficiency in the removal of metal ions [11]. According to the literature, a variety of natural and synthesized materials such as carbon active, clay, resin, zeolite, biomass, lignin and chitosan have been used as an adsorbent for the removal of heavy metals from aqueous solutions [12]. In recent years, magnetic nanoparticles (MNPs) have shown

*Corresponding author.

to be promising for the removal of heavy metal ions from aqueous solutions because no centrifugation and filtration is required. Furthermore, MNPs have premier features such as large removal capacity, fast kinetics and high reactivity and high surface area [13,14]. But some of the challenges that magnetic nanoparticles face is the susceptibility of consisted oxidize and dissolving easily, and also the recycling process is difficult due to the small size of nanoparticles. Finally, the MNPs tend to co-aggregate and cause reduction of the reaction activities and surface area limitation [15]. So MNPs functionalization is one of the best solutions to overcome these drawbacks [16]. Besides, surface modification techniques (physical or chemical) by different materials were used to reinforce the adsorption capacity and selectivity [17]. Many studies have been conducted regarding the surface improvement of MNPs by different functional groups for heavy metals removal. For example, Fe_3O_4 nanoparticle coated with talc exhibited effective removal of Cu(II), Ni(II), and Pb(II) ions from aqueous solutions [15]; magnetic nanoparticles impregnated onto tea waste (Fe_3O_4-TW) was developed for the highly efficient removal of Ni(II) from aqueous solutions [18]; iron oxide nanoparticles functionalized with starch was applied for the efficient adsorption of Cr(VI) from aqueous solutions [19]; amine-functionalized Fe_3O_4 used as an efficient agent to remove Cu(II) from aqueous solutions [20].

In most previous studies, the traditional methods of "one variable at a time (OVAT)" were used for optimization. This technique is not only timely, entails a lot of work and costly, but also cannot show the effect of interaction between different factors [11,21]. Response surface methodology (RSM) is a collection of mathematical and statistical techniques useful for studying the effect of several variables influencing the responses where its main objective is to determine the optimum condition of operational variables of the process [22].

The objectives of the present study is to investigate the synthesis of magnetic nanohybrid of Fe^{3+}-TMSPT-MNPs as a novel adsorbent and its application for the removal of Cr(VI) from aqueous solutions. Moreover, optimization of variables was conducted using central composite design (CCD) under response surface methodology (RSM) to get maximum removal efficiency (R). In this regard, the combined effect of sorbent dosage, pH and initial Cr(VI) concentrations on R as a response was investigated. The physicochemical characteristics of synthesized sorbent were evaluated by Fourier transform infrared (FT-IR), N_2 sorption-desorption, vibrating sample magnetometer (VSM), X-ray diffraction (XRD), and scanning electron microscopy (SEM). Moreover, Langmuir and Freundlich isotherms were applied to the equilibrium data to describe the main interactive mechanisms involved in the removal process. Kinetic parameters were also calculated from the pseudo-first-order and pseudo-second-order models. Furthermore, thermodynamic parameters (enthalpy, entropy and adsorption free energy), were calculated for a better description of the adsorption mechanism.

2. Materials and methods

2.1. Chemicals

Analytical grade ferric chloride hexahydrate ($FeCl_3{\cdot}6H_2O$), ferrous chloride tetrahydrate ($FeCl_2{\cdot}4H_2O$), ammonium hydroxide solution (25%), sodium hydroxide, hydrochloric acid, ethanol, n-Hexane, 2-propanol and 3-(trimethoxysilyl)-1-propanethiol were all purchased from Sigma-Aldrich and used without further purification. 1000 mL stock solution of Cr(VI) were prepared by dissolving potassium dichromate ($K_2Cr_2O_7$) in deionized water. Experimental solutions with the desired concentration were prepared by successive dilutions of the stock solution. Deionized distilled water was used in the preparation of all solutions.

2.2. Synthesis of magnetic Fe_3O_4 nanoparticles

Magnetic Fe_3O_4 nanoparticles (MNPs) were synthesized by the sol-gel method according to the literature [23]. In brief, firstly 5.2 g of $FeCl_3{\cdot}6H_2O$ and 2.0 g of $FeCl_2{\cdot}4H_2O$ were dissolved in the 200 mL deionized and deoxygenated water with mechanical stirring. Then under the protection of N_2 gas, 1.5 M (57.8 mL) of ammonium hydroxide solution (25%) was added dropwise into the above reaction mixture under vigorous stirring for 30 min. The resulting black nanoparticles were separated by an external magnetic field and for further purification were rinsed with deionized water three times. The collected black precipitate was dried in the oven at 50°C for 12 h.

2.3. Preparation of magnetic nanohybrid of Fe^{3+}-TMSPT-MNPs

The magnetic nanohybrid of Fe^{3+}-TMSPT-MNPs was prepared via the post-synthesis method for the first time. Briefly, 5 g of Fe_3O_4 was dispersed in 150 mL anhydrous n-Hexane. Then, under the protection of N_2 gas, 30 mmol of 3-(trimethoxysilyl)-1-propanethiol was added drop wise into the above reaction mixture. Then the mixture was refluxed at 70°C for 24 h and the product was separated by an external magnetic field, washed several times with n-hexane and dried in the oven at 50°C for 12 h. The product was represented as TMSPT-MNPs. In the second functionalization step, 5.21 g of as-synthesized TMSPT-MNPs was dispersed in the 100 mL 2-propanpl then 13.5 g of $FeCl_3{\cdot}6H_2O$ was added to the reaction mixture and refluxed at 30°C for 12 h. Finally, the magnetic nanohybrid of Fe^{3+}-TMSPT-MNPs was collected by an external magnetic field, washed several times with 2-propanpl and dried in the oven at 50°C for 12 h. Fig. 1 shows the schematic structure of Fe^{3+}-TMSPT-MNPs.

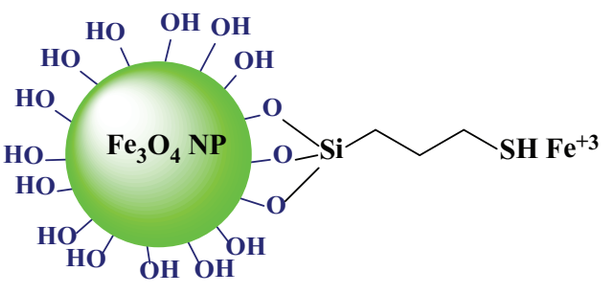

Fig. 1. Schematic structure of synthesized magnetic nanohybrid of Fe^{3+}-TMSPT-MNPs.

2.4. Characterization techniques

The produced materials were characterized by XRD, FT-IR, VSM, N_2 adsorption–desorption and SEM analyzes. The crystalline structures of the produced MNPs were examined by X-ray diffraction using GBC-Difftech MMA diffractometer. The nickel filtered Co Ka (λ = 1.54 A°) radiation was used at an acceleration voltage of 40 kV and current of 40 mA. The diffraction angle was scanned from 10 to 80 [2θ] at a rate of 18/min. Fourier transform infrared spectrometry (FT-IR) analyses were carried out on Bruker Vector 22 FT-IR Spectrometer in the range of 400–4000 cm^{-1} employing the KBr pellet method. Vibrating sample magnetometer (VSM) was employed to determine magnetic properties of synthesized materials (Lake Shore 7037/9509-P, USA). In order to determine the textural properties, the N_2 adsorption–desorption isotherms were measured using a 77 K by a Quantachrome Autosorb 1® volumetric analyzer. All of the samples were degassed at 50°C under an N_2 gas flow for 6 h before analysis. The specific surface area of the synthesized materials was evaluated using the Brunauer–Emmett–Teller (BET) method (P/P_0 = 0.02–0.98), and the pore size distribution was calculated from the desorption branch using the Barrett–Joyner–Halenda (BJH) method. The scanning electron microscopy (SEM) images were obtained with a microscope operating at 30 kV (SEM, MIRA3TESCAN, Czech Republic).

2.5. Batch adsorption procedure and modeling

The adsorption of Cr(VI) onto the Fe^{3+}-TMSPT-MNPs nanohybrid was investigated using batch experiments. Each experiment was carried out in 250 mL Erlenmeyer flasks containing 100 mL Cr(VI) solution by shaking the flasks for a contact period of 120 min. Samples were withdrawn at predetermined time intervals (0, 5, 10, 15, 30, 60, 90 and 120 min). All the adsorption experiments were carried out at room temperature of 25ºC. Cr(VI) stock solutions were prepared by dissolving potassium dichromate ($K_2Cr_2O_7$) powder in deionized water. The stock solution was diluted with de-ionized water to obtain the desired concentration range of Cr(VI) solutions. The pH of the Cr(VI) solutions was firstly adjusted using diluted HCl or NaOH solution before addition of the Fe^{3+}-TMSPT-MNPs nanohybrid. After adsorption reached equilibrium, the adsorbent was separated via an external magnetic field and the supernatant was collected for metal concentration measurements. Residual Cr(VI) concentration in the supernatant was determined by atomic adsorption spectrophotometer (Biotech, PHOENIX. 986 model). The removal efficiency (R) and adsorption capacity (q_e) were calculated according to the following equations [24]:

$$R = \frac{C_i - C_e}{C_i} \times 100 \quad (1)$$

$$q_e = \frac{V(C_i - C_e)}{S} \quad (2)$$

where, C_i and C_e are the initial and equivalent (residual) concentrations of Cr(VI) ions in $mg \cdot L^{-1}$, V is the volume of Cr(VI) containing solution in contact with the adsorbent in L, respectively, and S is the amount of added adsorbent on dry basis in g. All experiments were carried out in triplicate and the mean values were reported.

2.6. Central composite design

Optimum conditions for the adsorption of Cr(VI) were conducted based on a central composite design (CCD) and analyzed using response surface method (RSM). A CCD has three groups of design points including: a) two-level factorial or fractional factorial design points, b) axial points (sometimes called "star" points) and c) center points. CCD's are designed to estimate the coefficients of a quadratic model. All point descriptions will be in terms of coded values of the factors. Optimization studies were carried out by studying the effect of three variables, including Fe^{3+}-TMSPT-MNPs dosage, initial Cr(VI) concentrations and pH of the solutions. The selected independent variables used in this study were coded according to Eq. (3), [25]:

$$Z_i = \frac{X_i - X_0}{\Delta X} \quad (3)$$

where Z_i is the coded value of an independent variable, X_i is the actual value of an independent variable, X_0 is the actual value of an independent variable at the center point and ΔX is the value of step change. The actual values of process variables and their variation limits were selected based on the values obtained in the literature [22, 26–28] and coded as shown in Table 1.

As presented in Table 1, the experimental design involved three parameters (X_1, X_2 and X_3), each at five levels, coded –1, –α, 0, +α and +1, respectively. Factor ranges in term of (±1) levels selected by user (according to the literature) and factors in term of (±α) and (0) levels were selected by the software. Eight factorial points (±1), six axial points (±α) and six replicates at the center point (0) were chosen as experimental points. The removal efficiency (R) was given to software as an independent parameter (response). The following empirical second-order polynomial model (Eq. 4) explains the behavior of the system:

$$Y = a_0 + \sum_{(i=1)}^{n} a_i X_i + \sum_{(i=1)}^{n} a_i i X_i^2 + \sum_{(i=1)}^{(n-1)} \sum_{(j=2)}^{n} a_i j X_i X_j + \varepsilon \quad (4)$$

where Y is the predicted response, i and j are linear quadratic coefficients, a_0 is the intercept term, a_i is the linear coefficient, a_{ij} is the interactive coefficient, a_{ii} is quadratic coefficient, and ε is a random error [29]. The optimal values of the variables selected were obtained by the equation

Table 1
Independent variables and their coded levels for the central composite design (CCD)

Independent variables		Range and levels (coded)				
		−α	–1	0	+1	+α
pH	(X_1)	2.00	3.00	7.50	12.00	13.00
Sorbents dosage ($g \cdot L^{-1}$)	(X_2)	0.01	0.10	1.05	2.00	2.65
Cr(VI) concentration ($mg \cdot L^{-1}$)	(X_3)	2.50	5.00	52.50	100.00	132.39

regression and response surface curves. Twenty experiments were conducted according to the scheme mentioned in Table 2. The statistical significance of the variables, individual effect and interaction effects were evaluated on metal ion removal process by the analysis of variance (ANOVA). The quality of the fitted model was expressed by the coefficient of determination (R^2), and statistical significance was evaluated based on the p-value and F-value.

3. Results and discussion

3.1. Characterization of synthesized adsorbent

XRD analysis was used to investigate the crystalline structure of synthesized MNPs. Fig. 2 shows the X-ray diffraction patterns of the synthesized MNPs. It is consistent with the standard pattern in JCPDS file (65-3107). Seven characteristic peaks were observed in the XRD pattern at 2θ of 21.31°, 35.26°, 41.64°, 50.66°, 63.17°, 67.55°, and 74.47° (Fig. 2). These strong peaks ((111), (220), (311), (400), (422), (511), and (440)) confirmed that the products were well crystallized, which is in agreement with the results reported by Tan et al. and Li et al. [30,31]. The average particle size was calculated to be 10.80 nm using the Sherrer's equation Eq. (5) [32].

$$L = \frac{K * \lambda}{\beta * cos\theta} \quad (5)$$

where L is the average core diameter of particles (nm), K is grain shape factor ($K = 0.94$), λ is incident X-ray wavelength (nm), β is full width at half-maximum (FWHM) of the highest intensity 311 powder diffraction reflection (0.95), and θ is the corresponding diffraction angle ($2\theta = 41.64°$).

Fig. 3 shows the SEM images of MNPs with different magnifications. The shape of these particles was approximately spherical and appeared to be highly uniform. The comparison of the particles size estimated by Sherrer's

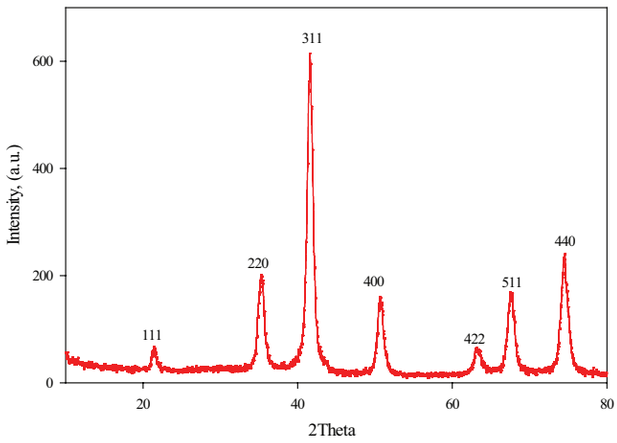

Fig. 2. X-ray diffraction pattern of synthesized MNPs.

Table 2
Experimental design in term of the coded factors and results of the CCD

Run number	Categorical factor levels	Independent values						Response (R%)	
		Real values			Coded values			Predicted value	Observed value
		X_1	X_2	X_3	X_1	X_2	X_3		
1	Factorial points	3.00	0.10	20.00	–1	–1	–1	25.25	25.89
2		11.00	0.10	5.00	1	1	–1	1.83	6.72
3		3.00	2.00	5.00	–1	1	–1	67.53	76.15
4		12.00	2.00	50.00	1	1	–1	15.00	14.66
5		4.00	0.10	100.00	–1	–1	1	8.80	13.12
6		5.00	0.10	80.00	1	–1	1	28.02	26.74
7	Axial points	8.00	2.00	100.00	–1	1	1	29.02	36.91
8		10.00	2.00	75.00	1	1	1	32.71	30.50
9		2.00	1.05	52.50	–α	0	0	33.18	32.15
10		13.00	1.05	52.50	+α	0	0	15.56	14.89
11		5.00	0.01	52.50	0	–α	0	33.25	28.81
12		2.00	2.65	52.50	0	+α	0	62.13	56.05
13		7.50	1.05	2.50	0	0	–α	31.79	21.03
14		9.00	1.05	132.39	0	0	+α	17.16	12.50
15	Central points	7.50	1.05	52.50	0	0	0	45.37	42.89
16		7.50	1.05	52.50	0	0	0	45.37	48.18
17		7.50	1.05	52.50	0	0	0	45.37	52.35
18		7.50	1.05	52.50	0	0	0	45.37	44.64
19		7.50	1.05	52.50	0	0	0	45.37	44.47
20		7.50	1.05	52.50	0	0	0	45.37	44.82

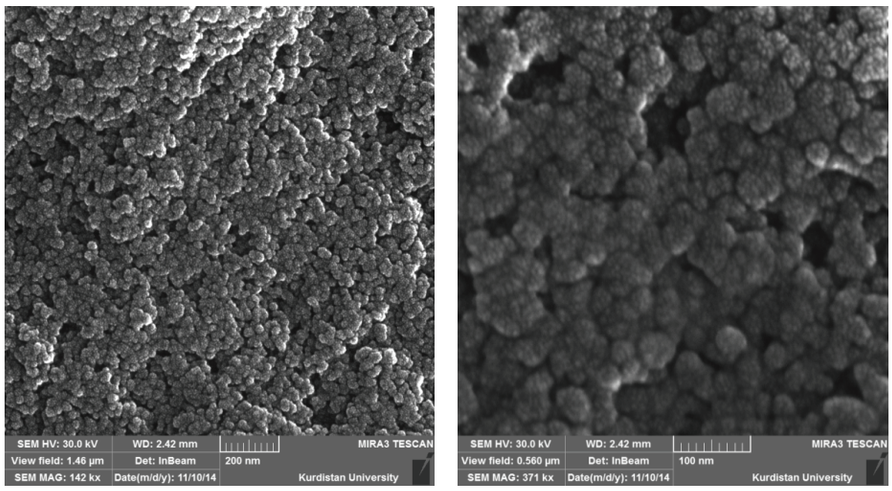

Fig. 3. SEM images of MNPs with different magnifications: a) ×142,000 and b) ×371,000.

equation with SEM results revealed that estimation of the MNPs size by SEM is difficult, because of the agglomeration and optical illusions.

Fig. 4 shows the FTIR spectra of MNPs and Fe^{3+}-TMSPT-MNPs in the wavenumber range 4000–400 cm^{-1}. The spectra displays a broad band at 568 cm^{-1} which is believed to be associated with the stretching vibrations of the tetrahedral groups (Fe^{3+}-O^{2-}) for Fe_3O_4. These results were similar to the Wang et al. study [33]. The band corresponding to –SH group in the spectrum of TMSPT-MNPs and Fe^{3+}-TMSPT-MNPs was not clearly observed (must be observed at 2551–2561 cm^{-1}) due to relative poor sensitivity of IR to the thiol group [13]. However, bands at 2920 and 2850 cm^{-1} attributed to the C–H stretch of methylene of the alkyl chain were obvious indicating TMSTP was successfully grafted to the surface of TMSPT-MNPs and Fe^{3+}-TMSPT-MNPs. On the other hand, the peaks around 1625 and 2856 cm^{-1} can be assigned to $–CH_2$ stretching mode and strong absorption band at 1100 cm^{-1}, resulting from the vibration of Si-O-Si that confirmed the grafting of silica network on to the MNPs [34].

The magnetic properties of the synthesized materials were investigated at room temperature (300°K). Fig. 5 shows them agnetization curve of MNPs, TMSPT-MNPs and Fe^{3+}-TMSPT-MNPs with the external field sweeping between ±8 k Oe at room temperature. It can be seen that the saturated magnetization (Ms) values were found to be 65.40, 62.80 and 48.47 emu/g^{-1} for MNPs, TMSPT-MNPs and Fe^{3+}-TMSPT-MNPs, respectively. Besides, the three magnetization curves go through the zero point and overlap each other (that means that the values of the magnetizability and coercivity of the sample are zero) [35]. All manifest the super paramagnetic nature of the MNPs, TMSPT-MNPs and Fe^{3+}-TMSPT-MNPs samples with no magnetic hysteresis.

The textural features of the synthesized MNPs, TMSPT-MNPs and Fe^{3+}-TMSPT-MNPs samples were determined by the N_2 adsorption-desorption analysis. Physical parameters of nitrogen isotherms containing the BET surface area (S_{BET}) and the total pore volumes (V_{total}) of the synthesized samples are summarized in Table 3. The surface area of an

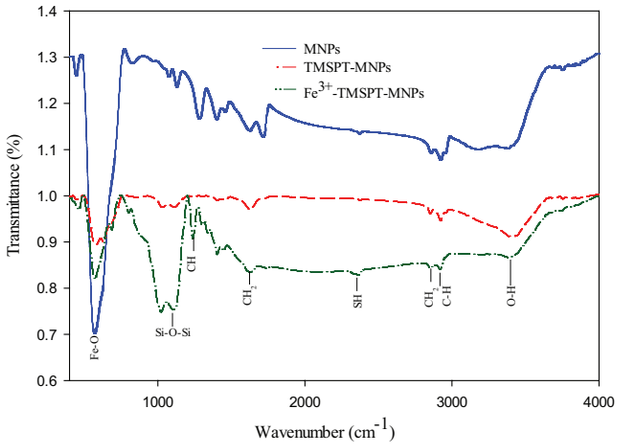

Fig. 4. FTIR spectra of MNPs, TMSPT-MNPs and Fe^{3+}-TMSPT-MNPs.

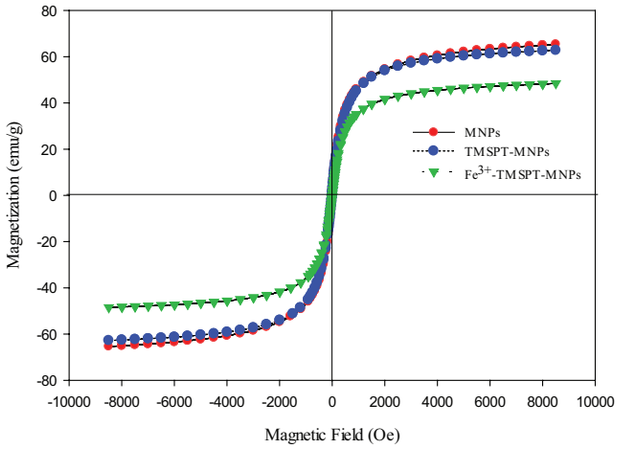

Fig. 5. Magnetization curves of MNPs, TMSPT-MNPs and Fe^{3+}-TMSPT-MNPs.

Table 3
Textural properties of MNPs, TMSPT–MNPs and Fe^{3+}–TMSPT–MNPs

Sample	S_{BET} (m^2/g)	V_{total} (cm^3/g)
MNPs	89.99	0.33
TMSPT–MNPs	62.65	0.21
Fe^{3+}–TMSPT–MNPs	57.5	0.17

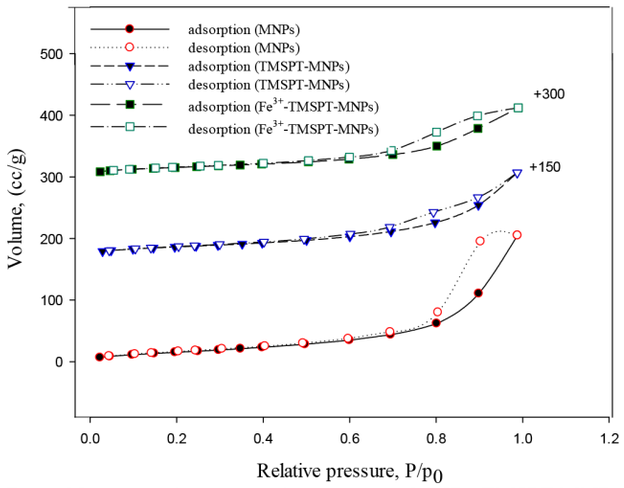

Fig. 6. Nitrogen adsorption–desorption of MNPs, TMSPT-MNPs and Fe^{3+}-TMSPT-MNPs.

adsorbent is one of the important structural parameters that can determine its adsorption efficiency. The obtained result revealed that after functionalization, a decrease in the surface area (S_{BET}) was observed. It can be due to the presence of functional groups on the surface that can partially block the adsorption of N_2 molecules. The results of N_2 adsorption–desorption measurements for MNPs, TMSPT-MNPs and Fe^{3+}-TMSPT-MNPs are presented in Fig. 6.

3.2. Evaluation of adsorption potential by MNPs, TMSPT-MNPs and Fe^{3+}-TMSPT-MNPs

In order to evaluate and comparison of the adsorbent efficiency and adsorption capacity, the effect of MNPs, TMSPT-MNPs and Fe^{3+}-TMSPT-MNPs on the adsorption of Cr(VI) at three test run with pH 5, sorbent dosage of 0.1 $g{\cdot}L^{-1}$ and Cr(VI) concentration 80 $mg{\cdot}L^{-1}$ were studied. The obtained results revealed that the removal efficiency (R) of Cr(VI) by MNPs, TMSPT-MNPs and Fe^{3+}-TMSPT-MNPs increased from 13.27% to 20.01% and 25.49% after functionalization by TMSPT and Fe^{3+} at the same conditions, respectively (Fig. 7). In addition, the Cr(VI) adsorption capacity (q_e) of MNPs, TMSPT-MNPs and Fe^{3+}-TMSPT-MNPs were 106.17, 160.08 and 203.95 $mg{\cdot}g^{-1}$, respectively. As demonstrated in Fig. 7, Fe^{3+}-TMSPT-MNPs adsorbent has much higher Cr(VI) removal efficiency and adsorption capacity compared to TMSPT-MNPs and MNPs, which referred to the grafted thiol and Fe^{+3} groups on the surface of magnetic nanoparticles and its more active adsorption sites. Therefore Fe^{3+}-TMSPT-MNPs was chosen as an appropriate adsorbent for optimization of the other parameters.

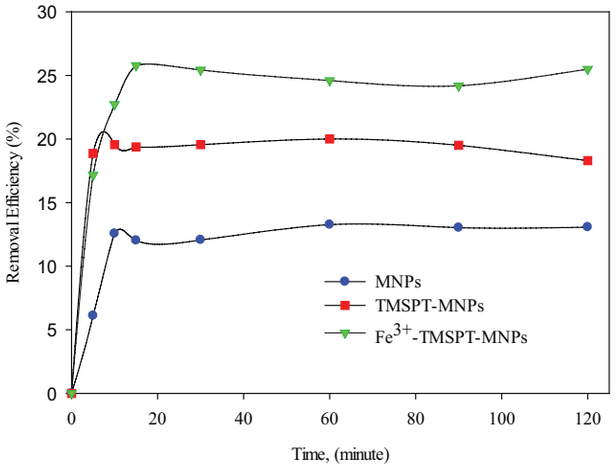

Fig. 7. Comparison of Cr(VI) removal efficiency potentials by MNPs, TMSPT-MNPs and Fe^{3+}-TMSPT-MNPs.

3.3. Fitting of process models and statistical analysis

The CCD was used to develop a polynomial regression equation to determine the interactions of selected variables on the adsorption of Cr (VI). The analysis of variance (ANOVA) was used to determine the main and interaction effects of independent variables on Cr(VI) adsorption onto the Fe^{3+}-TMSPT-MNPs, the results of which are given in Table 4. The relationship between the removal of chromium ions and the independent variables was obtained by quadratic model (Eq. (6)):

$$R = +3.96 + 6.95 * X_1 + 33.78 * X_2 + 0.06 * X_3 - 2.73 * X_1 * X_2 + 0.09 * X_1 * X_3 - 0.15 * X_2 * X_3 - 0.69 * X_1^2 - 0.53 * X_2^2 - 5.47E-3 * X_3^2 \quad (R^2 = 0.925) \quad (6)$$

The significance of the quadratic model coefficients was evaluated by the F-value and p-values and sum of square (SS) listed in Table 4. The effect of each factor was statistically significant at $P < 0.05$ and also quantifies sum of squares (SS) of each factor is important in the process and as the value of the SS increases the significance of the corresponding factor in the undergoing process also increases [17]. The larger magnitude of the F-value (13.67) and the p-value less than 0.05 demonstrate that model terms are significant for the sorption of Cr(VI). The correlation coefficient (R^2) is found to be 0.925, indicates the better fitness of the model in the experimental data. On the basis of quadratic equation of response surface methodology [Eq. (6)], the effect of independent variables: pH, sorbents dosage and initial ion concentrations on the adsorption of Cr(VI) were analyzed. As demonstrated in Eq. (6), each three variables have a positive effect on the removal of Cr(VI), it means that the removal of Cr(VI) increased as the pH, sorbent dosage and ion concentrations increased. Initial solution pH compared to the other variables has the most influential and significant effect on the adsorption process ($p = 0.0434$, SS = 238.52, F = 5.34). The actual and predicted removal efficiency plot for Cr(VI) is displayed in Fig. 8. The actual values were the measured response data for a particular run [estimated experimentally by Eq. (1)], and the

Table 4
Regression analysis using response surface quadratic model for *R* response

Term	Sum of squares	Degrees of freedom	Mean square	F–value	P–value
Model	5489.99	9	610.00	13.67	0.0002
X_1	238.52	1	238.52	5.34	0.0434
X_2	61.04	1	61.04	1.37	0.2693
X_3	0.039	1	0.039	8.79E–4	0.9769
X_1X_2	622.55	1	622.55	13.95	0.0039
X_1X_3	567.14	1	567.14	12.71	0.0051
X_2X_3	193.40	1	193.40	4.33	0.0640
X_1^2	828.55	1	828.55	18.57	0.0015
X_2^2	1.27	1	1.27	0.028	0.8694
X_3^2	914.55	1	914.55	20.49	0.0011
Residual	446.25	10	44.62		
Lack of fit	386.17	5	77.23	6.43	0.0311
Pure error	60.07	5	12.01		
Cor. total	5936.24	19			

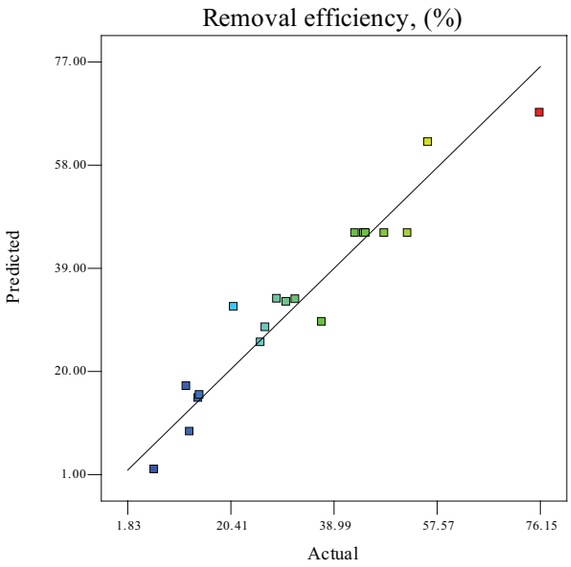

Fig. 8. Correlation of actual and predicted values for removal efficiency.

predicted values of *R* were evaluated from the models and generated by using the approximating functions [generated by Eq. (6)]. It indicated that the predicted values obtained by the model and the actual experimental data were in good agreement. Generally, this methodology could be successful in studying the importance of individual, cumulative, and interactive effects of the process variables in adsorption.

3.4. 3D response surface and contour plots

Fig. 9a–c demonstrate the three dimensional and contour plots for evaluation of interaction effects between pH, initial Cr(VI) concentration and sorbent dosage for Cr(VI) ion removal.

3.4.1. Effect of initial pH

To investigate the combined effect of pH with sorbent dosage and initial Cr(VI) concentration, the RSM was used and the results were presented in the form of 3D and contours plots (Fig. 9a and b). The pH of the solution is an important factor in the adsorption process, which affects surface charge of the adsorbent by their functional group and chromium speciation in the solution. It seems that at acidic conditions, chromium ions exists in different forms including $HCrO_4^-$, $Cr_2O_7^-$, $Cr_3O_{10}^{2-}$, $Cr_4O_{13}^{2-}$ and when the pH of the solution increases predominant species were CrO_4^{2-} and $Cr_2O_7^{2-}$ [36]. As seen in Fig. 9 a and b, the removal efficiency of Cr(VI) increased with the increasing of solution pH from 2 until 4.28, and decreases when the pH value is higher than 5. At low pH (pH < 5) predominating form of Cr(VI) in solution is $HCrO_4^-$ and the $-Fe^{3+}$ groups on the sorbent surface were protonated and possess positive electric. Hence, electrostatic attraction between positively charged sorbent surface and negatively charged chromium species increased and finally leads to increasing removal efficiency of Cr(VI). According to the literature, chromium adsorption by different sorbents was higher at acidic conditions [19,36–38]. For example, Parsons et al. [7] used the magnetite nanoparticles for the removal of Cr(III) and Cr(VI). Their results revealed that the best pH for adsorption of Cr(VI) was 4.

3.4.2. Effect of initial Cr(VI) concentration

The results of the mutual effect of initial Cr(VI) concentration with pH and sorbent dosage are presented in Fig. 9b and c. It can be observed that the removal efficiency decreased as the initial Cr(VI) concentration increased. Since in the high concentrations, the adsorption sites saturated and the number of available adsorption sites decreased. Also it may be concluded that at a lower concentration, the ratio of available surface to the initial Cr(VI) concentration is larger, therefore, the removal is higher [37].

3.4.3. Effect of sorbent dosage

The mutual effect of sorbent dosage with pH and initial Cr(VI) concentration has been presented in Fig. 9a and c. It can be observed that the removal efficiency improved with an increase in the sorbent dosage. Actually, with the increase of sorbent dosage, more surface area was available for adsorption due to the increase in the number of active binding sites. A similar type of result has also been observed by other researchers [26,39]. As can be seen from Table 4, all the p-values of X_1, X_1^2, X_3^2, X_1X_2, and X_1X_3 are less than 0.05, which indicates that these variables are significant and have great influence on Cr(VI) adsorption.

3.5. Process optimization

One of the main aims of this study was to find the optimum process parameters to maximize the removal efficiency (R) of Cr(VI) by the developed mathematical models.

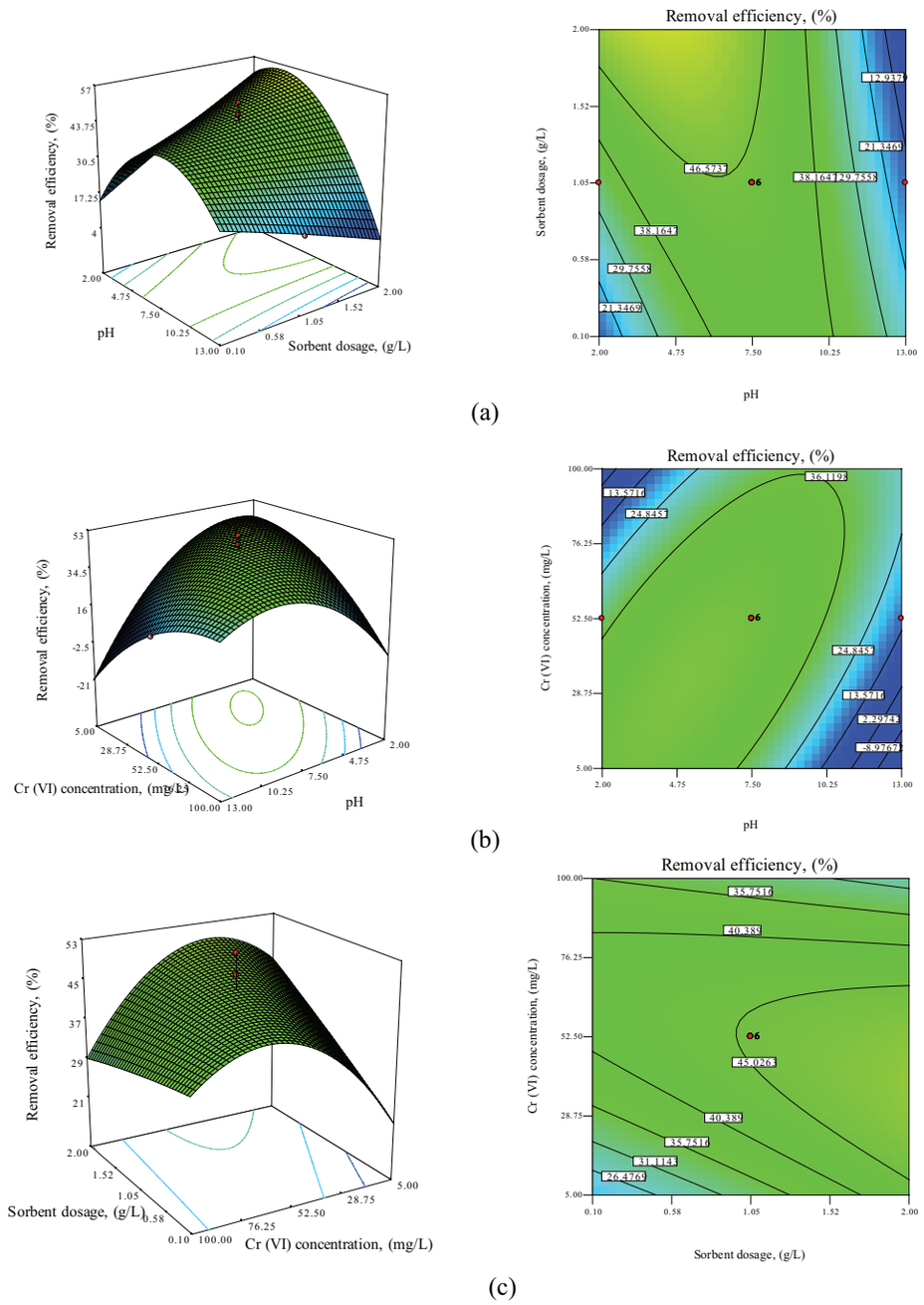

Fig. 9. 3D surface and contour plots for chromium removal efficiency at 120 min showing the mutual effect of: a) pH and sorbent dosage, b) pH and Cr(VI) concentration, c) sorbent dosage and Cr(VI) concentration.

The process parameters were optimized using numerical optimization option in the software in a manner that the desired goal for each factor and response was selected from the menu. The possible goals are: maximize, minimize, target, within range, none (for responses only) and set to an exact value (factors only). The goals are composed into an overall desirability function. In the numerical optimization, we choose the desired goal for each factor and response from the menu. Optimum values of the selected variables were obtained by analyzing the response surface 3D and contour plots and solving the regression equation. A multiple response method was applied for optimizing any combination of the four goals, namely the initial solution pH, initial Cr(VI) concentration, sorbent dosage, and removal efficiency (R). The optimum values of every factor and desirability ramps are shown in Fig. 10. These charts show the slope of changes for variables. The numerical optimization found a point that maximizes the desirability function.

In this study, numerical optimization using RSM led to the optimum operating condition as pH of 4.28, initial Cr (VI) concentration of 30 mg·L^{-1} and sorbent dosage of 2 g·L^{-1} with desirability of 0.945. The obtained value of desirability (0.945) shows that the estimated function may represent the experimental model and desired conditions. It can be concluded that CCD statistical design was effective in determining the optimum conditions for Cr(VI) adsorption onto Fe^{3+}-TMSPT-MNPs as an adsorbent.

3.6. Adsorption kinetics

The adsorption kinetic data obtained from batch experiments were analyzed using a pseudo-first-order and pseudo-second-order that these models most often used to analyze the rate of adsorption. The pseudo-first order and pseudo-second order models can be expressed as Eqs. (7) and (8), respectively [40]:

$$\ln\left(q_e - q_t\right) = \ln q_e - k_1 t \tag{7}$$

$$\frac{t}{q_t} = \frac{1}{k_2 q_e^2} + \frac{t}{q_e} \tag{8}$$

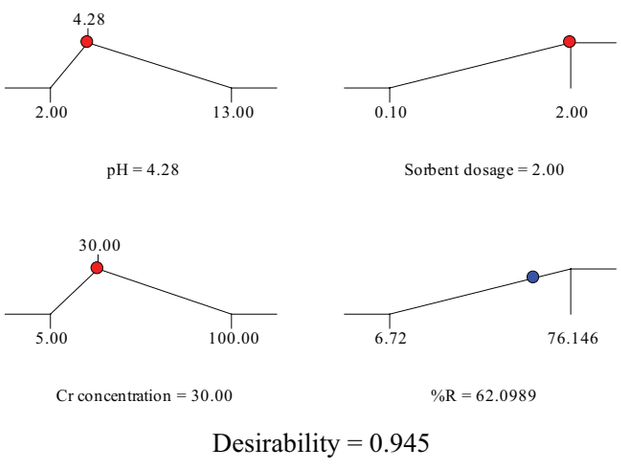

Fig. 10. Desirability ramps for numerical optimization of four goals, namely the initial solution pH, sorbent dosage, initial Cr(VI) concentration and removal efficiency (R).

where q_e and q_t are the amounts of metal ions adsorbed on to Fe^{3+}-TMSPT-MNPs at equilibrium and at time t (mg·g^{-1}), respectively, and k_1 (min^{-1}), k_2 (g·mg^{-1}·min^{-1}) are the equilibrium rate constants for pseudo first order and pseudo second order adsorption. Additionally, and k_1 parameters for the pseudo first order kinetic model were calculated from intercept and slope linear plots of versus t (min) and for pseudo second order kinetic model parameters q_e and k_2 were calculated from slope and intercept linear plots of $t{\cdot}q_t^{-1}$ (min·g·mg^{-1}) versus t. The estimated kinetic models and related parameters with linear regression coefficient (R^2) are shown in Table 5. As demonstrated in this table, the correlation coefficients of the pseudo-second order equation, in all of the Cr(VI) concentrations are near to 1 and significantly higher than that for the pseudo-first order equation. The theoretical q_e (q_{e2}) values for metal ions were also very close to the values construed from the experiment (q_e^{exp}). These observations suggest that adsorption kinetics followed the pseudo-second-order equation, indicating that the chemical sorption as the rate-limiting step of adsorption mechanism [41,42].

3.7. Adsorption isotherms

The adsorption isotherm describes the equilibrium of the sorption of a material on the surface. Adsorption isotherms were used to determine the binding capacities for Cr(VI) to the Fe^{3+}-TMSPT-MNPs adsorbent. Two different isotherms that are widely used to describe the adsorption processes are Langmuir and Freundlich isotherms. The Langmuir model assumes that the uptake occurs on a homogeneous surface with a finite number of identical sites and has been applied successfully in many monolayer adsorption processes [20,43]. The Langmuir isotherm model has the following form [44]:

$$q_e = \frac{q_{\max} b C_e}{1 + b C_e} \tag{9}$$

where q_e is the amount of Cr(VI) adsorbed at equilibrium in (mg·g^{-1}), C_e is the equilibrium metal concentration in (mg·L^{-1}), q_m is the maximum adsorption capacity in (mg·g^{-1}), and b is the Langmuir constant (L·mg^{-1}) referred to adsorption energy. In other words, b is a constant related to the affinity of binding sites with the metal ions. The Freundlich model, an empirical equation used to describe heterogeneous adsorption systems, can be represented as follows [5]:

Table 5
Kinetic parameters for the adsorption rate expressions

C_i, mg·L^{-1}	$q_e^{exp.}$mg·g^{-1}	Pseudo–first–order			Pseudo–second–order		
		q_{e1}, mg·g^{-1}	$-K_1$, min^{-1}	R^2	q_{e2}, mg·g^{-1}	K_2, min^{-1}	R^2
5	6.962	5.748	0.087	0.883	7.07	0.574	0.998
25	21.53	9.333	0.065	0.624	34.01	0.330	0.933
50	33.37	19.104	0.035	0.794	34.01	0.141	0.996
80	42.61	15.439	0.015	0.354	37.31	–0.071	0.994
100	45.77	13.69	0.149	0.671	44.05	–0.037	0.989

C_i: initial Cr (VI) concentration; $q_e^{exp.}$: experimental value; q_{e1} and q_{e2}: calculated values; K_1 and K_2: rate constants.

$$q_e = k_f C_e^{1/n} \quad (10)$$

where k_f (mg·g^{-1}) and n (L·mg^{-1}) are the Freundlich constants related to adsorption capacity and intensity, respectively. The Langmuir and Freundlich parameters and their correlation coefficients (R^2) evaluated by plotting q_e versus C_e (Fig. 11) are given in Table 6. The comparison of obtained R^2 values for both models in Table 3 reveals that adsorption of Cr(VI) by Fe^{3+}-TMSPT-MNPs adsorbent follows the Freundlich isotherm model. Therefore the experimental data fit very well to this isotherm model and indicate that adsorption of Cr(VI) occurs follows multilayer and heterogeneous adsorption process. Table 6 also presents that n value is greater than 1.0, reflects that the adsorption of Cr(VI) on the adsorbents is favorable. The maximum adsorption capacity (q_{max}) of Cr(VI) on adsorbent calculated from Langmuir adsorption isotherm was 128.65 mg·g^{-1} which shows a stronger binding of Cr (VI) on adsorbent.

3.8. Thermodynamic studies

The thermodynamics is important in understanding the adsorption and designing better adsorption parameters. In thermodynamic studies, the determination of standard enthalpy (ΔH^o), standard free energy (ΔG^o) and standard entropy (ΔS^o) is necessary. The thermodynamic parameters can be determined using the distribution coefficient (K) that is dependent on temperature. The change in Gibbs free energies (ΔG) were then calculated with Eq. (11). ΔH and ΔS were calculated from the slope and intercept of the plot of versus 1/T using Eq. (12). In addition, the distribution coefficient (K) was calculated from the concentration of Cr(VI) in the initial concentration (C_i) and equilibrium concentration (C_e) according to the Eq. (13), [42,45]:

$$\Delta G = \Delta H - T\Delta S \quad (11)$$

$$lnk = \frac{\Delta s}{R} - \frac{\Delta H}{RT} \quad (12)$$

$$K = \frac{C_0 - C_e}{C_e} * \frac{V}{m} \quad (13)$$

where, R is the universal gas constant (8.314 J/mol K) and T (°K) is the solution temperature. The parameters of ΔH^o and ΔS^o, can be obtained from the slope and intercept of plots (ln k versus 1/T), respectively. V is the volume of the solution (mL) and m is the mass of the sorbent (g). Temperature has a direct influence on the adsorption process. The adsorption experiments were conducted in the temperature range of 293–323°K. The values of thermodynamic parameters such as ΔG^o, ΔH^o, ΔS^o, describing Cr(VI) uptake by Fe^{3+}-TMSPT-MNPs adsorbent that were calculated using mentioned above Eqns. (11–13). All the thermodynamic parameters are listed in Table 7 and the thermodynamic curves of Cr(VI) adsorption shows in Fig. 12. It was observed that Cr(VI) adsorption increased with increasing temperature. The negative value ΔH^o confirms that the sorption process was exothermic in nature. The negative values of ΔG^o at all temperatures illustrate the feasibility and spontaneous nature

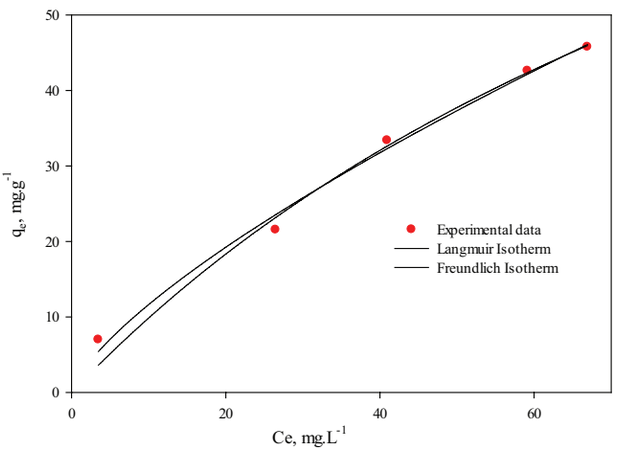

Fig. 11. Langmuir and Freundlich isotherms for adsorption of Cr(VI) ions on Fe^{3+}-TMSPT-MNPs.

Table 6
Constants of Langmuir and Freundlich isotherms for Cr(VI) ions adsorption by Fe^{3+}–TMSPT–MNPs

Langmuir			Freundlich		
q_{max}	b	R^2	K_f	n	R^2
128.65	0.008	0.986	2.198	1.381	0.992

Table 7
Thermodynamic parameters of Cr(VI) adsorption on Fe^{3+}–TMSPT–MNPs at different temperatures in Kelvin (initial concentration of Cr(VI) ions was 60 mg·L^{-1})

–ΔH°, J/mol	ΔS°, J/mol·K	–ΔG°, kJ/mol				R^2
		293°K	303°K	313°K	323°K	
25.40	138.91	40.73	42.12	43.50	44.89	0.921

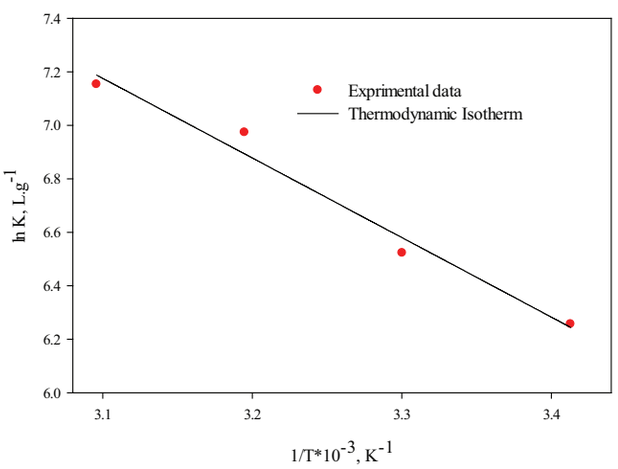

Fig. 12. Plot of ln$K$ vs. 1/T × 10^{-3} for estimation of thermodynamic parameters for Cr(VI) adsorption.

of adsorption process. As can be seen, the values of ΔG were decreased with an increase in temperature that shows the reaction is more feasible at a higher temperature. The positive value of ΔS^o indicated the affinity of Cr(VI) for the Fe^{3+}-TMSPT-MNPs and thus the disorderliness prevails.

3.9. Sorbent regeneration and competing ions study

Sorbent regeneration studies help to elucidate the adsorption mechanism and recovery of metal-loaded adsorbent, hence may be able to reduce operational cost and protect the environment [46]. In the present study,desorption of Cr(VI) ions from loaded Fe^{3+}-TMSPT-MNPs was carried out using 0.3 M HCL solutions in four successive adsorption-desorption cycles with sorbent dosage of 0.15 g·L^{-1}, pH level of 4.28 and Cr (VI) concentration 60 mg·L^{-1} by the following method. The Cr (VI)-loaded Fe^{3+}-TMSPT-MNPs nanohybrid was separated and stirred with HCL 0.3 M solutions for 6 h at room temperature. Then the adsorbent was washed with deionized water and was dried in the oven at 50°C for 12 h. When the Cr(VI)-loaded Fe^{3+}-TMSPT-MNPs sorbent was added to the HCL solution, the H^+ ions begin replacing with Cr(VI) ions on the sorbent surface. In the other words, if Cr(VI) was adsorbed on Fe^{3+} binding groups by electrostatic interaction, then acid solutions would regenerate the adsorbent surface since the concentration of H^+ ions increases and thus leads to ion exchange with the chromium adsorbed [47]. As evident from the results (Fig. 13), the removal efficiency of Cr(VI) does not noticeably change during the four reactive cycles. Therefore, the results suggest that the Fe^{3+}-TMSPT-MNPs adsorbent has an excellent reusability and is cost effective for the removal of Cr(VI).

The removal efficiency of Cr(VI) was compared with several inorganic elements including Cu(II), Mn(II), Zn(II), Fe(II), As(V), Pb(II), Cd(II) and Ni(II) at the ideal conditions (Table 8). The obtained results revealed that in all of the evaluated elements there is not significant interference on Cr(VI) adsorption, except with As(V). It seems that As(V) shows a chemical behavior similar to that of Cr(VI) ions and can be a serious competitor in adsorption process. This is in further accordance with kinetic studies of Cr(VI) and As(V) sorption in binary mixtures reported by previous study [48].

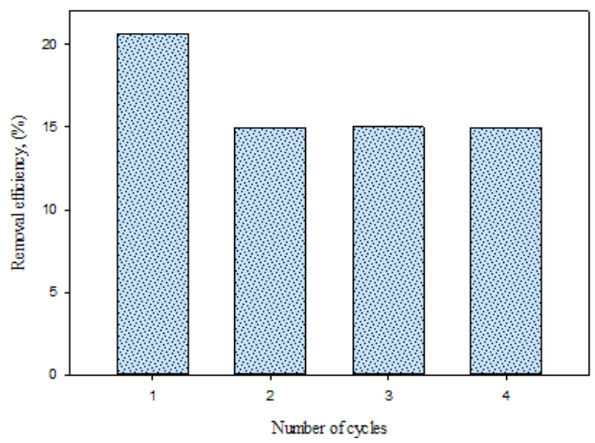

Fig. 13. W Regeneration studies of Fe^{3+}-TMSPT-MNPs nanohybrid after four cycles.

Table 8
Effect of competing ions on Cr(VI) removal efficiency with pH 4.28, sorbent dosage of 2 g·L^{-1} and ions concentration 30 mg·L^{-1} were studied

	Removal efficiency (%)
Cu(II)	0
Mn(II)	0
Zn(II)	2.14
Fe(II)	0
As(V)	71.65
Pb(II)	1.13
Cd(II)	2.17
Ni(II)	0
Cr(VI)	62.09

4. Conclusion

In this study, removal of Cr(VI) ions by Fe^{3+}-TMSPT-MNPs was investigated and optimal conditions of process parameters and maximum Cr(VI) removal efficiency was found using central composite design under response surface methodology. The ANOVA results demonstrate that the selected quadratic model with p-value of <0.05 was significant for the experimental data. The value of R^2 = 0.945 for the obtained quadratic model indicates the high correlation between experimental values and predicted values. Numerical optimization using RSM led to the optimum operating condition as pH of 4.28, Cr(VI) concentration of 30 mg·L^{-1} and sorbent dosage of 2 g·L^{-1} yielding Cr(VI) removal of 62.1%. Adsorption isotherms followed the multilayer adsorption and pseudo-second-order kinetic model fits well with the adsorption data obtained for Cr(VI) adsorptions. The calculated thermodynamic parameters indicated the feasible, spontaneous and endothermic nature of the adsorption process. Moreover, the adsorbed Cr(VI) was readily desorbed with HCl solution and the sorbents exhibited good reusability.

References

[1] G. Bayramoglu, M. Yakuparica, Adsorption of Cr(VI) onto PEI immobilized acrylate-based magnetic beads: Isotherms, kinetics and thermodynamics study, Chem. Eng. J., 139 (2008) 20–28.
[2] C.E. Barrera-Díaz, V. Lugo-Lugo, B. Bilyeu, A review of chemical, electrochemical and biological methods for aqueous Cr(VI) reduction, J. Hazard. Mater., 223–224 (2012) 1–12.
[3] D. Krishna, K.S. Krishna, R.P. Sre, Response surface modeling and optimization of chromium(VI) removal from aqueous solution using borasus flabellifer coir powder., Int. J. Appl. Sci. Eng., (2013) 213–226.
[4] V.K. Gupta, A. Rastogi, A. Nayak, Adsorption studies on the removal of hexavalent chromium from aqueous solution using a low cost fertilizer industry waste material, J. Colloid. Interf Sci., 342 (2010) 135–141.
[5] H.I. Adegoke, F. AmooAdekola, O.S. Fatoki, B.J. Ximba, Adsorption of Cr (VI) on synthetic hematite (α-Fe_2O_3) nanoparticles of different morphologies, Korean. J. Chem. Eng., 31 (2013) 142–154.

[6] B. Kakavandi, R.R. Kalantary, M. Farzadkia, A.H. Mahvi, A. Esrafili, A. Azari, A.R. Yari, A.B. Javid, Enhanced chromium (VI) removal using activated carbon modified by zero valent iron and silver bimetallic nanoparticles, J. Environ. Health. Sci. Eng., 12 (2014) 115.
[7] J.G. Parsons, J. Hernandez, C.M. Gonzalez, J.L. Gardea-Torresdey, Sorption of Cr(III) and Cr(VI) to high and low pressure synthetic nano-magnetite (FeO) Particles, Chem. Eng. J., 254 (2014) 171–180.
[8] G. Tiravanti, D. Petruzzelli, R. Passino, Pretreatment of tannery wastewaters by an ion exchange process for Cr(III) removal and recovery, Water. Sci. Technol., 36 (1997) 197–207.
[9] T. Olmez, The optimization of Cr(VI) reduction and removal by electrocoagulation using response surface methodology, J. Hazard. Mater., 162 (2009) 1371–1378.
[10] A.K. Chakravarti, S.B. Chowdhury, S. Chakrabarty, T. Chakrabarty, D.C. Mukherjee, Liquid membrane multiple emulsion process of chromium(VI) separation from waste waters, Colloid. Surface. A., (1995) 59–71.
[11] S. Sugashini, K.M.M.S. Begum, Optimization using central composite design (CCD) for the biosorption of Cr(VI) ions by cross linked chitosan carbonized rice husk (CCACR), Clean. Technol. Envir., 15 (2012) 293–302.
[12] S.E. Bailey, T.J. Olin, R.M. Bricka, D.D. Adrian, A review of potentially low-cost sorbents for heavy metals, Water. Res., 33 (1999) 2469–2479.
[13] S. Zhang, Y. Zhang, J. Liu, Q. Xu, H. Xiao, X. Wang, H. Xu, J. Zhou, Thiol modified Fe_3O_4@SiO_2 as a robust, high effective, and recycling magnetic sorbent for mercury removal, Chem. Eng. J., 226 (2013) 30–38.
[14] S.C. Tang, I.M. Lo, Magnetic nanoparticles: essential factors for sustainable environmental applications, Water. Res., 47 (2013) 2613–2632.
[15] K. Kalantari, M. Ahmad, H. Masoumi, K. Shameli, M. Basri, R. Khandanlou, Rapid adsorption of heavy metals by Fe_3O_4/Talc Nanocomposite and optimization study using response surface methodology, Int. J. Mol. Sci., 15 (2014) 12913–12927.
[16] C.Y. Haw, F. Mohamed, C.H. Chia, S. Radiman, S. Zakaria, N.M. Huang, H.N. Lim, Hydrothermal synthesis of magnetite nanoparticles as MRI contrast agents, Ceram. Int., 36 (2010) 1417–1422.
[17] R. Gottipati, S. Mishra, Process optimization of adsorption of Cr(VI) on activated carbons prepared from plant precursors by a two-level full factorial design, Chem. Eng. J., 160 (2010) 99–107.
[18] P. Panneerselvam, N. Morad, K.A. Tan, Magnetic nanoparticle (Fe_3O_4) impregnated onto tea waste for the removal of nickel(II) from aqueous solution, J. Hazard. Mater., 186 (2011) 160–168.
[19] P.N. Singh, D. Tiwary, I. Sinha, Improved removal of Cr(VI) by starch functionalized iron oxide nanoparticles, J. Environ. Chem. Eng., 2 (2014) 2252–2258.
[20] Y.M. Hao, C. Man, Z.B. Hu, Effective removal of Cu (II) ions from aqueous solution by amino-functionalized magnetic nanoparticles, J. Hazard. Mater., 184 (2010) 392–399.
[21] S. Sharma, A. Malik, S. Satya, Application of response surface methodology (RSM) for optimization of nutrient supplementation for Cr (VI) removal by Aspergillus lentulus AML05, J. Hazard. Mater., 164 (2009) 1198–1204.
[22] K.P. Singh, A.K. Singh, S. Gupta, S. Sinha, Optimization of Cr(VI) reduction by zero-valent bimetallic nanoparticles using the response surface modeling approach, Desalination, 270 (2011) 275–284.
[23] J. Hu, G. Chen, I.M. Lo, Removal and recovery of Cr(VI) from wastewater by maghemite nanoparticles, Water. Res., 39 (2005) 4528–4536.
[24] R. Kumar, R. Singh, N. Kumar, K. Bishnoi, N.R. Bishnoi, Response surface methodology approach for optimization of biosorption process for removal of Cr (VI), Ni (II) and Zn (II) ions by immobilized bacterial biomass sp. Bacillus brevis, Chem. Eng. J., 146 (2009) 401–407.
[25] M. Amini, H. Younesi, N. Bahramifar, A.A.Z. Lorestani, F. Ghorbani, A. Daneshi, M. Sharifzadeh, Application of response surface methodology for optimization of lead biosorption in an aqueous solution by Aspergillus niger, J. Hazard. Mater., 154 (2008) 694–702.
[26] B. Singha, S.K. Das, Biosorption of Cr(VI) ions from aqueous solutions: Kinetics, equilibrium, thermodynamics and desorption studies, Colloid. Surface. B., 84 (2011) 221–232.
[27] M. Demirel, B. Kayan, Application of response surface methodology and central composite design for the optimization of textile dye degradation by wet air oxidation, Int. J. Ind. Chem., 3 (2012) 1–10.
[28] A.R. Esfahani, A.F. Firouzi, G. Sayyad, A. Kiasat, L. Alidokht, A.R. Khataee, Pb(II) removal from aqueous solution by polyacrylic acid stabilized zero-valent iron nanoparticles: process optimization using response surface methodology, Res. Chem. Intermediat., 40 (2014) 431–445.
[29] R. Yongsheng, L. Jun, D. Xiaoxiao, Application of the central composite design and response surface methodology to remove arsenic from industrial phosphorus by oxidation, Can. J. Chem. Eng., 89 (2011) 491–498.
[30] C. Li, Y. Wei, A. Liivat, Y. Zhu, J. Zhu, Microwave-solvothermal synthesis of Fe_3O_4 magnetic nanoparticles, Mater. Lett., 107 (2013) 23–26.
[31] Y. Tan, M. Chen, Y. Hao, High efficient removal of Pb (II) by amino-functionalized Fe_3O_4 magnetic nano-particles, Chem. Eng. J., 191 (2012) 104–111.
[32] V.K. Gupta, S. Agarwal, T.A. Saleh, Chromium removal by combining the magnetic properties of iron oxide with adsorption properties of carbon nanotubes, Water. Res., 45 (2011) 2207–2212.
[33] L. Wang, J. Li, Q. Jiang, L. Zhao, Water-soluble Fe_3O_4 nanoparticles with high solubility for removal of heavy-metal ions from waste water, Dalton. Trans., 41 (2012) 4544–4551.
[34] S.A. Idris, S.R. Harvey, L.T. Gibson, Selective extraction of mercury(II) from water samples using mercapto functionalised-MCM-41 and regeneration of the sorbent using microwave digestion, J. Hazard. Mater., 193 (2011) 171–176.
[35] J. Meng, G. Yang, L. Yan, X. Wang, Synthesis and characterization of magnetic nanometer pigment Fe_3O_4, Dyes. Pigments., 66 (2005) 109–113.
[36] M. Jain, V.K. Garg, K. Kadirvelu, Adsorption of hexavalent chromium from aqueous medium onto carbonaceous adsorbents prepared from waste biomass, J. Environ. Manage., 91 (2010) 949–957.
[37] Y. Pang, G. Zeng, L. Tang, Y. Zhang, Y. Liu, X. Lei, Z. Li, J. Zhang, Z. Liu, Y. Xiong, Preparation and application of stability enhanced magnetic nanoparticles for rapid removal of Cr(VI), Chem. Eng. J., 175 (2011) 222–227.
[38] P. Yuan, M. Fan, D. Yang, H. He, D. Liu, A. Yuan, J. Zhu, T. Chen, Montmorillonite-supported magnetite nanoparticles for the removal of hexavalent chromium [Cr(VI)] from aqueous solutions, J. Hazard. Mater., 166 (2009) 821–829.
[39] C.S. Jeon, K. Baek, J.K. Park, Y.K. Oh, S.D. Lee, Adsorption characteristics of As(V) on iron-coated zeolite, J. Hazard. Mater., 163 (2009) 804–808.
[40] X. Yu, S. Tong, M. Ge, L. Wu, J. Zuo, C. Cao, W. Song, Synthesis and characterization of multi-amino-functionalized cellulose for arsenic adsorption, Carbohyd. Polym., 92 (2013) 380–387.
[41] J. Cao, Y. Wu, Y. Jin, P. Yilihan, W. Huang, Response surface methodology approach for optimization of the removal of chromium(VI) by NH_2-MCM-41, J. Taiwan. Inst. Chem. Eng., 45 (2014) 860–868.
[42] F. Ghorbani, H. Younesi, Z. Mehraban, M. Sabri Celik, A.A. Ghoreyshi, M. Anbia, Aqueous Cadmium ions removal by adsorption on APTMS Grafted Mesoporous Silica MCM-41 in batch and fixed bed column processes, Int. J. Eng., 26 (2013).
[43] A. Gupta, M. Yunus, N. Sankararamakrishnan, Zerovalent iron encapsulated chitosan nanospheres - a novel adsorbent for the removal of total inorganic arsenic from aqueous systems, Chemosphere, 86 (2012) 150–155.

[44] C. Jing, Z. Zhaoxiang, X. Hong, Y. Zhong, C. Rizhi, Fabrication of Poly(ã-glutamic acid)-coated Fe_3O_4 Magnetic nanoparticles and their application in heavy metal removal, Chinese Chem. Eng. J., 21 (2013) 1244—1250.
[45] S.-Y. Yoon, C.-G. Lee, J.-A. Park, J.-H. Kim, S.-B. Kim, S.-H. Lee, J.-W. Choi, Kinetic, equilibrium and thermodynamic studies for phosphate adsorption to magnetic iron oxide nanoparticles, Chem. Eng. J., 236 (2014) 341–347.
[46] D. Wankasi, M. Horsfall Jnr, A. Spiff, Desorption of Pb^{2+} and Cu^{2+} from Nipa palm (Nypa fruticans Wurmb) biomass, Afr. J. Biotechnol., 4 (2005) 923–927.
[47] G.R. Bernardo, R.M. Rene, A.D. Ma Catalina, Chromium (III) uptake by agro-waste biosorbents: chemical characterization, sorption-desorption studies, and mechanism, J. Hazard. Mater., 170 (2009) 845–854.
[48] M. Aryal, M. Ziagova, M. Liakopoulou-Kyriakides, Comparison of Cr(VI) and As(V) removal in single and binary mixtures with Fe(III)-treated Staphylococcus xylosus biomass: Thermodynamic studies, Chem. Eng. J., 169 (2011) 100–106.